



# Influence of the crystal structure of $\text{Ag}_2\text{CO}_3$ on the photocatalytic activity under visible light of $\text{Ag}_2\text{CO}_3$ -Palygorskite nanocomposite material

Omar Lakbita, Benaïssa Rhouta, Francis Maury, François Senocq, M'Barek Amjoud, Lahcen Daoudi

## ► To cite this version:

Omar Lakbita, Benaïssa Rhouta, Francis Maury, François Senocq, M'Barek Amjoud, et al.. Influence of the crystal structure of  $\text{Ag}_2\text{CO}_3$  on the photocatalytic activity under visible light of  $\text{Ag}_2\text{CO}_3$ -Palygorskite nanocomposite material. Applied Surface Science, 2019, 464, pp.205-211. 10.1016/j.apsusc.2018.09.053 . hal-01879719

**HAL Id: hal-01879719**

**<https://hal.science/hal-01879719>**

Submitted on 24 Sep 2018

**HAL** is a multi-disciplinary open access archive for the deposit and dissemination of scientific research documents, whether they are published or not. The documents may come from teaching and research institutions in France or abroad, or from public or private research centers.

L'archive ouverte pluridisciplinaire **HAL**, est destinée au dépôt et à la diffusion de documents scientifiques de niveau recherche, publiés ou non, émanant des établissements d'enseignement et de recherche français ou étrangers, des laboratoires publics ou privés.






OATAO is an open access repository that collects the work of Toulouse researchers and makes it freely available over the web where possible

This is an author's version published in: <http://oatao.univ-toulouse.fr/20811>

**Official URL:** <https://doi.org/10.1016/j.apsusc.2018.09.053>

**To cite this version:**

Lakbita, Omar  and Rhouta, Benaïssa and Maury, Francis   
and Senocq, François  and Amjoud, M'barek and Daoudi,  
Lahcen *Influence of the crystal structure of Ag<sub>2</sub>CO<sub>3</sub> on the  
photocatalytic activity under visible light of Ag<sub>2</sub>CO<sub>3</sub>-  
Palygorskite nanocomposite material.* (2019) Applied Surface  
Science, 464. 205-211. ISSN 0169-4332

Any correspondence concerning this service should be sent  
to the repository administrator: [tech-oatao@listes-diff.inp-toulouse.fr](mailto:tech-oatao@listes-diff.inp-toulouse.fr)

# Influence of the crystal structure of $\text{Ag}_2\text{CO}_3$ on the photocatalytic activity under visible light of $\text{Ag}_2\text{CO}_3$ -Palygorskite nanocomposite material

O. Lakbita<sup>a,b</sup>, B. Rhouta<sup>a,\*</sup>, F. Maury<sup>b</sup>, F. Senocq<sup>b</sup>, M. Amjoud<sup>a</sup>, L. Daoudi<sup>c</sup>

<sup>a</sup> Laboratoire de Matière Condensée et Nanostructures (LMCN), Faculté des Sciences et Techniques Guéliz, Université Cadi Ayyad, BP 549, Marrakech, Morocco

<sup>b</sup> CIRIMAT, Université de Toulouse, CNRS-UPS-INP, ENSIACET, 4 allée Emile Monso, BP 44362, 31030 Toulouse cedex 4, France

<sup>c</sup> Laboratoire de Géoscience et Géoenvironnement, Faculté des Sciences et Techniques Guéliz, Université Cadi Ayyad, BP 549, Marrakech, Morocco

## ABSTRACT

In a companion paper, it has been demonstrated the remarkably beneficial effect of palygorskite clay (Pal) fibers as support material coupled to appropriate thermal treatments and aging under  $\text{CO}_2$  atmosphere in monitoring the phase composition of  $\text{Ag}_2\text{CO}_3$ -Pal composite. In this new nanocomposite material, the structure of the functional component  $\text{Ag}_2\text{CO}_3$  can be controlled from 100% stable monoclinic (m) to 100% metastable hexagonal  $\beta$  through an adjusted mixture of m- and  $\beta$ - $\text{Ag}_2\text{CO}_3$ . The present study deals with the assessment of the visible photocatalytic properties of these various nanocomposite materials towards the removal of Orange G dye from aqueous solutions. It was found that the  $\text{Ag}_2\text{CO}_3$ -Pal nanocomposite in which  $\text{Ag}_2\text{CO}_3$  was single-phased and crystallized with the stable monoclinic structure was more active than the one crystallizing entirely with the metastable  $\beta$ - $\text{Ag}_2\text{CO}_3$  structure. Nevertheless, the composite material containing a mixture of both  $\text{Ag}_2\text{CO}_3$  phases with a relative content of 32% of  $\beta$ - and 68% of m-phase was found to be the most photoactive compound of the series. This behavior reveals likely a synergetic effect between both phases in the photocatalytic degradation of the dye under visible light.

## 1. Introduction

Over the past decades, heterogeneous photocatalysis has emerged as an efficient alternative process for the degradation of organic and bioorganic pollutants in wastewater. Besides its low cost and high stability,  $\text{TiO}_2$  is the most investigated and used compound because it is one of the most photoactive materials. It was reported that  $\text{TiO}_2$  in the form of anatase is more photoactive than the one in the form rutile [1]. However, the coexistence of both allotropes in specific proportions, e.g. anatase (80%) and rutile (20%) as in commercial  $\text{TiO}_2$  nanopowder Degussa P25 is responsible of a higher photocatalytic activity under UV light. This results from a synergetic action between both phases, and justifies its worldwide use in wastewater treatment [2,3]. However, because of the easy agglomeration of  $\text{TiO}_2$  nanoparticles (NPs), the photocatalytic activity of such nano-powder decreases over times for most degradation processes [4] leading to a need to implement costly microfiltration processes for recovering micrometric sized aggregates from water decontaminated by  $\text{TiO}_2$  slurry [1,2,5,6]. It follows a great interest for new photocatalysts that avoid this problem.

To overcome this issue, several works have been recently devoted to the immobilization of  $\text{TiO}_2$  NPs on monolithic supports designed and

manufactured for obtaining large surface areas such as glass fibers [7], cotton fibers [8], beads [9,10], membranes [11,12] and silica micro-fiber fabrics [13,14], or on different powdered and porous materials like silica gels [15,16], zeolites [17], activated carbons [2,18,19] and clay minerals [3,4,20–24]. In this respect, we have reported in several papers [25–28] the beneficial effect of natural clayey supports such as stevensite, palygorskite and beidellite to avoid large grain growth, sintering and agglomeration of  $\text{TiO}_2$  nanoparticles during their synthesis. Also, the extraordinary stabilization of the metastable photoactive anatase phase at high temperature ( $\approx 900^\circ\text{C}$ ) was found, which is an advantage for possible regeneration processes of the photocatalyst. As a result, these nanocomposites exhibited UV photocatalytic activity much higher than that of pure Degussa P25 for a same amount of  $\text{TiO}_2$ . Nevertheless, the photoactivity of  $\text{TiO}_2$  supported clay photocatalysts is effective only under UV radiations due to the large energy band gap of the semiconductor oxide. Therefore, the development of highly visible-light driven photocatalysts always raises a great interest.

In this respect, despite the issue of its sensitivity to photo-corrosion [29–32], silver carbonate ( $\text{Ag}_2\text{CO}_3$ ) was reported to exhibit highly efficient photoactivity under visible light [30,32–35]. Also, Ag-based compounds are well known for antibacterial activity [36–38]. In this

context, in the ancient Greece, it was customary to place silver coins in water to inhibit bacterial growth [36]. Therefore it is a good candidate as multi-functional material, *i.e.* combining both antibacterial and photocatalytic properties. For this purpose, novel supported nanocomposite photocatalysts based on  $\text{Ag}_2\text{CO}_3$  in replacement of  $\text{TiO}_2$  as active phase and palygorskite clay mineral as support material, were successfully synthesized as described in details in a companion paper [39]. The beneficial effect of the surface of palygorskite fibers has been shown to refine  $\text{Ag}_2\text{CO}_3$  particles size and to stabilize its metastable hexagonal  $\beta$ -phase. Besides, the combination of appropriate thermal treatments and aging under  $\text{CO}_2$  atmosphere allowed to control the phase composition of  $\text{Ag}_2\text{CO}_3$ /Pal nanocomposites, in which  $\text{Ag}_2\text{CO}_3$  crystal structure ranges from stable monoclinic single-phase ( $\alpha$ ) to 100% metastable  $\beta$ -phase through a mixture of  $\alpha$ - and  $\beta$ - $\text{Ag}_2\text{CO}_3$  with various proportions in Pal-based composite material.

The present work aims at studying the effect of the phase composition of  $\text{Ag}_2\text{CO}_3$ /Pal supported nanocomposites on their photocatalytic properties as a function of the crystal structure and the relative content of  $\text{Ag}_2\text{CO}_3$  phases under visible light towards the removal of Orange G dye, selected as a model pollutant of wastewater.

## 2. Experimental

### 2.1. Starting materials

The palygorskite used in this study was isolated from natural clay picked up from Marrakech High Atlas region, Morocco, and exchanged with  $\text{Na}^+$  (labeled  $\text{Na}^+$ -Pal) according to respective purification and homoionization procedures described in details elsewhere [25,40,41]. Briefly, an aqueous dispersion of a given mass of raw clay was reacted with hydrochloric solution (1 M) at  $\text{pH} = 4$  to remove carbonate impurities. The dispersion was centrifuged and the solid was washed several times till the supernatant  $\text{pH}$  reached 7. The solid was thereafter treated under stirring for 24 h by  $\text{NaCl}$  solution (2 M). This operation was repeated twice to ensure a complete exchange of the charge compensating cations by  $\text{Na}^+$ . The treated clay was recovered by repetitive washing with distilled water until free of chloride, as confirmed by the  $\text{AgNO}_3$  test. The fine fraction (particle size  $< 2 \mu\text{m}$ ) was separated from the 5 wt% dispersion, according to Stokes' law [42]. This operation was repeated several times till the dispersion was almost transparent. The homoionic sodium palygorskite  $\text{Na}^+$ -Pal was recovered by centrifugation at 4000 rpm (*i.e.*  $1073 \times g$ ) for 20 min and dried at 353 K.

Previous characterizations performed by Rhouta et al. [40] showed that this palygorskite is predominantly dioctahedral, deficient in zeolitic water and associated with 5 wt% of sepiolite. The composition of this palygorskite was found on the basis of 26 oxygen atoms to be  $(\text{Si}_{7.97}\text{Al}_{0.03})(\text{Mg}_{2.17}\text{Al}_{1.46}\text{Fe}_{0.40}\text{Ti}_{0.05})(\text{Ca}_{0.03}\text{Na}_{0.07}\text{K}_{0.03})\text{O}_{20.18}(\text{OH})_{1.94}(\text{H}_2\text{O})_{3.88}, 2.43 \text{ H}_2\text{O}$ . Its CEC (Cation Exchange Capacity), BET specific surface area and total porous volume were assessed to be  $21.2 \text{ meq} \cdot 100 \text{ g}^{-1}$ ,  $116 \text{ m}^2 \cdot \text{g}^{-1}$ , in which external surface is around  $88 \text{ m}^2 \cdot \text{g}^{-1}$ , and  $0.458 \text{ cm}^3 \cdot \text{g}^{-1}$  respectively.

The other starting compounds  $\text{AgNO}_3$  and  $\text{Na}_2\text{CO}_3$  involved in the syntheses and Orange G dye for photocatalytic tests were purchased from Aldrich and used as received without further purification.

### 2.2. Preparation of $\text{Ag}_2\text{CO}_3$ -Pal nanocomposites

Several Pal- $\text{Ag}_2\text{CO}_3$  composites with different  $\text{Ag}_2\text{CO}_3$  contents were synthesized by an easy and simple wet route. For preparing composites containing X wt% of  $\text{Ag}_2\text{CO}_3$  ( $X = 10, 20, 42, 57, 67$  and  $80 \text{ wt\%}$ ) (labeled Pal-X% $\text{Ag}_2\text{CO}_3$ ), 0.5 g of  $\text{Na}^+$ -Pal was first dispersed under ultrasounds for 15 min in 20 mL of  $\text{AgNO}_3$  aqueous solution of a given concentration (Table 1). This dispersion was maintained under stirring for 1 h in the dark. Thereafter, 40 mL of  $\text{Na}_2\text{CO}_3$  aqueous solution of a given concentration was slowly added dropwise under stirring to the

**Table 1**

Molar concentrations of  $\text{AgNO}_3$  and  $\text{Na}_2\text{CO}_3$  solutions used in the preparation of Pal-X% $\text{Ag}_2\text{CO}_3$  nanocomposite materials. The corresponding amount of  $\text{Ag}^+$  involved in these preparations is given in equivalent of CEC of palygorskite.

Pal/X% $\text{Ag}_2\text{CO}_3$ X (%)	$\text{AgNO}_3$ (M)	$\text{Na}_2\text{CO}_3$ (M)	$\text{Ag}^+$ equiv. CEC (Pal)
10	0.040	0.010	3.3
20	0.090	0.023	8.0
42	0.260	0.065	23.5
57	0.500	0.130	45.5
68	0.770	0.190	70.0
80	1.450	0.360	182.0

dispersion for 15 min. As shown in Table 1, it is worth noting that the amount of  $\text{Ag}^+$  involved in the preparation of Pal- $\text{Ag}_2\text{CO}_3$  composites is in excess with respect to cationic exchange capacity of palygorskite found to be  $21.2 \text{ meq} \cdot 100 \text{ g}^{-1}$  [40]. The mixture was kept under stirring at ambient temperature and in the dark for either 1 h (protocol 1) or 24 h (protocol 2) of digestion period, in the same way than the procedure reported by Nagy et al. [43]. These authors indeed demonstrated a difference in  $\text{Ag}_2\text{CO}_3$  reactivity depending on the digestion duration. Accordingly, the composite materials were designated as Pal-X % $\text{Ag}_2\text{CO}_3$ -1 h or Pal-X% $\text{Ag}_2\text{CO}_3$ -24 h respectively. A yellow precipitate, obtained in both conditions of digestion, was recovered by centrifuging at 5000 rpm (*i.e.*  $1677 \times g$ ) for 15 min, washed several times with deionized water and thereafter centrifuged twice by using deionized water, and once by using ethanol to remove reaction byproducts. Finally, the powdered material obtained was dried in an oven at  $60^\circ\text{C}$  for 48 h and stored in the dark for further uses.

Pure  $\text{Ag}_2\text{CO}_3$  was also synthesized according to the protocol 1 using the same conditions as above but without the palygorskite clay mineral. More details on the synthesis of these composite materials is reported in a companion paper [39]. These experimental protocols, completed with others after aging are summarized in Table 2.

### 2.3. Characterization methods and techniques

X-ray diffraction (XRD) patterns were recorded at room temperature and ambient atmosphere on pure  $\text{Ag}_2\text{CO}_3$  and on  $\text{Ag}_2\text{CO}_3$ -Pal composite samples in  $2\theta$  range  $3\text{--}80^\circ$  with an acquisition step of  $0.02^\circ$  at a rate of  $2 \text{ s/step}$  using a Bruker D8-2 diffractometer equipped with a graphite monochromator (Bragg-Brentano configuration;  $\text{Cu K}_\alpha$  radiation).

The monoclinic-hexagonal phase transformation of  $\text{Ag}_2\text{CO}_3$  was investigated by *in situ* XRD as a function of the temperature under  $\text{CO}_2$  atmosphere. Different samples prepared with and without palygorskite as support material were analyzed in the  $2\theta$  range  $15\text{--}40^\circ$  using a Bruker D8 Advance diffractometer equipped with a Lynx Eye® detector and a MRI radiation heating chamber (Bragg-Brentano configuration;  $\text{Ni}$  filtered  $\text{Cu K}_\alpha$  radiation). The XRD chamber was purged with  $\text{CO}_2$  prior the experiment. The measurements were made under a low  $\text{CO}_2$  flow rate ( $50 \text{ sccm}$ ) to maintain a slight overpressure close to atmospheric pressure. For pure  $\text{Ag}_2\text{CO}_3$ , the diffractograms were recorded every  $25^\circ\text{C}$  from 50 to  $235^\circ\text{C}$ . An isotherm was maintained at each level for 10 min to record the XRD pattern and then the temperature was increased to the next step using a ramp of  $1 \text{ deg} \cdot \text{s}^{-1}$  as explained in details

**Table 2**

Synthesis protocols of Pal-57% $\text{Ag}_2\text{CO}_3$  composite materials used to control the relative content  $\beta/(m + \beta)$  of the metastable  $\beta$ -hexagonal phase from 0 to 100%. The common steps (CS) of all protocols are described in the text.

Protocol	Experimental procedure	Duration	$\beta$ - $\text{Ag}_2\text{CO}_3$ content (%)
# 1	CS// Stirring-RT-in the dark	1 h	32
# 2	CS// Stirring-RT-in the dark	24 h	0
# 3	Protocol #1 + Aging/1 cycle $\text{CO}_2$ @ $200^\circ\text{C}$	6 months/1h	100

in a companion paper [39].

In order to investigate if it was possible to control the proportion of each  $\text{Ag}_2\text{CO}_3$  phases in the composite samples by appropriate heat treatments under  $\text{CO}_2$  atmosphere, as well as to study the aging of the photocatalyst, a series of XRD patterns were recorded at room temperature after specific thermal cycles under  $\text{CO}_2$  atmosphere. Typically a composite sample Pal-57% $\text{Ag}_2\text{CO}_3$  underwent two heating cycles at 210 °C with an isothermal step at this temperature for 1 h in the first cycle and 5 h in the second one, then a cooling to 50 °C after each heating. The sample was maintained at 50 °C for 12 h between the two cycles. Finally, a last XRD pattern was recorded 60 h later after storage under  $\text{CO}_2$  atmosphere in the dark at 50 °C (protocol 3). In an attempt to form pure hexagonal  $\beta$ -phase, the Pal-57% $\text{Ag}_2\text{CO}_3$  composite sample as-prepared according to protocol 1 was stored in the dark at the ambient and XRD patterns were recorded after 6 and 7 months of aging. The sample was thereafter, heated under  $\text{CO}_2$  atmosphere for 1 h at 200 °C before performing an *in situ* XRD analysis. At the end, the sample was cooled down to 50 °C and a last XRD pattern was recorded (protocol 4). All these treatments are illustrated in a parallel paper [39] and they are summarized in Table 2.

A Jeol JSM 6400 scanning electron microscope (SEM) equipped with an Oxford energy dispersive spectrometer, EDS (Si–Li detector; MK program) and a JEOL JEM 2100F transmission electron microscopy (TEM) equipped with a Bruker AXS Quantax EDS analyzer were used for characterizing clay particles and performing local elemental analysis on nanocomposite samples.

#### 2.4. Photocatalytic tests

The photocatalytic activity of different samples was evaluated by measuring the decomposition rate of OG in aqueous solutions containing a dispersion of the photocatalyst in a batch lab-scale reactor either under visible or UV irradiations. This anionic dye compound was selected as model pollutant because its adsorption onto clay minerals was negligible due to electrostatic repulsion between negatively charged clay particles and dye anionic entities [44]. The degradation reaction was carried out in a quartz vessel ( $40 \times 20 \times 36 \text{ mm}^3$ ) transparent to wavelengths  $> 290 \text{ nm}$  which was placed in a thermostated chamber (25 °C).

Photocatalytic tests under visible light were performed by using 4 lightcolor/840 lamps coupled with a UV cut-off filter (400 nm). These visible lamps have an electric power of 52 W and they provide a cumulative irradiance near 550 nm of  $3 \text{ mW} \cdot \text{cm}^{-2}$ . This photon flux was obtained by adjusting the distance between the reactor and the lamps at about 15 cm.

The photocatalytic tests under UV were performed using the same protocol but using a HPLN Philips 125 W lamp emitting at 365 nm. This UV lamp was chosen because the OG absorption is negligible at this wavelength and consequently the direct photolysis of the OG solution (without photocatalyst) was found negligible for more than 24 h. The reactor was irradiated with a photon flux of  $1 \text{ mW} \cdot \text{cm}^{-2}$  by adjusting the distance to the lamp to simulate the UV intensity of solar spectrum on the earth [45].

The photocatalyst powder was added to  $25 \text{ cm}^3$  of OG solution ( $10^{-5} \text{ M}$ ) in an amount equal to  $1 \text{ g} \cdot \text{dm}^{-3}$ . This catalyst mass was considered to be an optimum to avoid excess of catalyst and to ensure an efficient absorption of photons [2,46]. Before UV or visible irradiation, all dispersions were agitated for 1 h in the dark to reach adsorption equilibrium with the photocatalyst using an inert Teflon magnetic stirrer. Then the agitation was maintained during the test under irradiation. To determine the dye concentration, aliquots were taken from the mixture at regular time intervals using a syringe equipped with  $0.2 \mu\text{m}$  filter. The OG concentration in the supernatant was determined by measuring the absorbance at 480 nm using a UV–VIS–NIR spectrophotometer (Perkin Elmer lambda 19) and by applying the Beer Lambert's law.

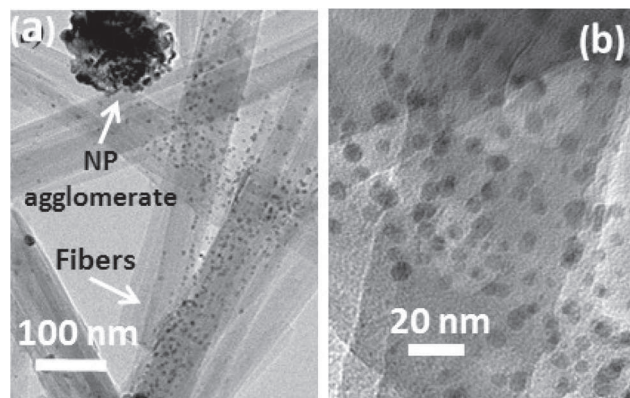


**Fig. 1.** TEM micrographs of a Pal-57% $\text{Ag}_2\text{CO}_3$  composite sample showing (a) a porous agglomerate ( $\approx 100 \text{ nm}$ ) of  $\text{Ag}_2\text{CO}_3$  NPs retained by the entanglement of fibers resulting from nucleation in homogeneous phase and (b) the heterogeneous growth of  $\text{Ag}_2\text{CO}_3$  NPs ( $< 10 \text{ nm}$ ) dispersed on the surface of palygorskite fibers.

### 3. Results and discussion

#### 3.1. The metastable $\beta$ - $\text{Ag}_2\text{CO}_3$ phase

Recently we have reported the remarkable effect of fibrous palygorskite clay mineral in the stabilization at room temperature of the metastable hexagonal  $\beta$ - $\text{Ag}_2\text{CO}_3$  phase along with the usual stable monoclinic  $m$ -phase and the refinement of their particles size ( $< 10 \text{ nm}$ ). Growth of  $\beta$ - $\text{Ag}_2\text{CO}_3$  likely originates from heterogeneous mechanism that occurs on the surface of palygorskite fibers. This growth mode would compete with homogenous nucleation taking place in aqueous solution and leading to  $m$ - $\text{Ag}_2\text{CO}_3$  NPs, which tends to form nodular and porous agglomerates trapped in tangled fibers. Both growth mechanisms would occur simultaneously [39]. The  $\beta$ - $\text{Ag}_2\text{CO}_3$  was not observed by TEM analyses probably because it is unstable under electronic impact. TEM images of pure  $\beta$ - $\text{Ag}_2\text{CO}_3$  were reported recently for porous  $\text{Ag}_2\text{CO}_3$  nanorods but no electronic diffraction result was given to confirm that the structural transformation did not take place [47]. However, in our case, Fig. 1 gives evidence for two types of  $\text{Ag}_2\text{CO}_3$  NPs in agreement with this mechanism.

All support materials do not stabilize the  $\beta$ -phase. For instance, using celite [39] or  $\text{C}_3\text{N}_4$  [48],  $\text{Ag}_2\text{CO}_3$  keeps the monoclinic structure. Also, metastable phases can be stabilized by the nanometric size of the particles produced by the growth mechanism. Thus, a synthesis method of pure  $\text{Ag}_2\text{CO}_3$  (without support) produced nanorods of  $\beta$ - $\text{Ag}_2\text{CO}_3$  (10 nm) [47].

The relative content of  $\beta$ - $\text{Ag}_2\text{CO}_3$  in supported nanocomposites can be increased by post-treatments until to reach 100% as summarized in Table 2. These protocols demonstrate an easy phase transformation between  $m$ - and  $\beta$ -structure.

This structural transformation is entirely reversible only for pure  $\text{Ag}_2\text{CO}_3$  while it is not if the  $\beta$ -phase is stabilized as for instance by the surface of palygorskite. Thus, this reversibility was demonstrated for pure  $\text{Ag}_2\text{CO}_3$  by *in situ* XRD as a function of the temperature under  $\text{CO}_2$  atmosphere; the formation of  $\beta$ - $\text{Ag}_2\text{CO}_3$  occurring at about 180 °C [39] in agreement with other authors [49–54]. In this series of *in situ* XRD patterns, the strongest diffraction peak (1 3 0) of  $m$ - $\text{Ag}_2\text{CO}_3$  at  $2\theta \approx 33.7^\circ$  is not shifted by increasing the temperature until it disappears beyond 200 °C to form a high temperature phase (Fig. 2a). No network expansion due to thermal expansion occurs in this crystallographic direction. This lattice plane (1 3 0) was assumed to be the most exposed and active plane in photocatalysis [55] but it does not seem to play a role in  $m/\beta$  structural change.

By contrast, the second reflection in intensity ( $-1\ 0\ 1$ ) at  $2\theta \approx 32.6^\circ$  of the monoclinic phase is shifted towards small angles before vanishing



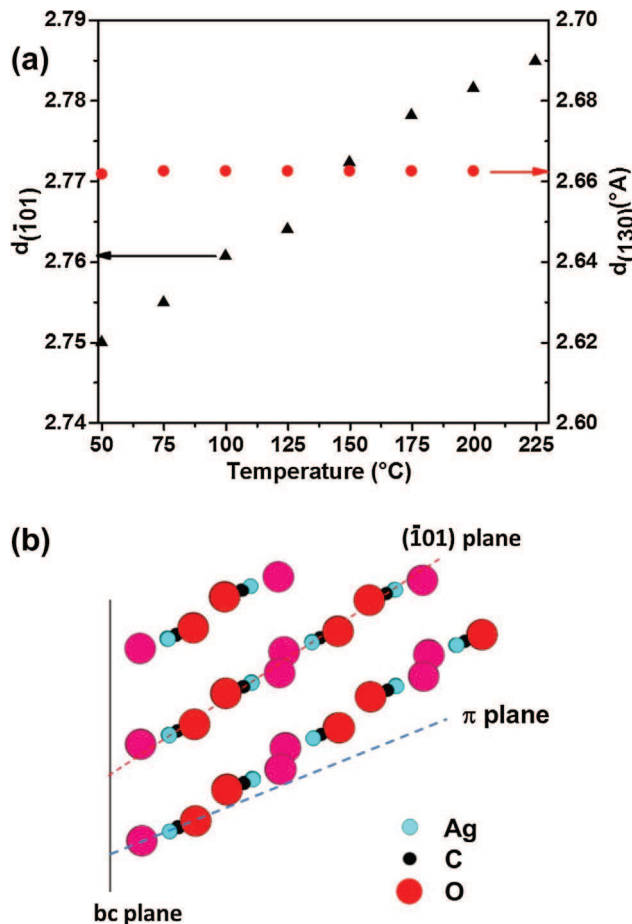


Fig. 2. (a) variation of the interplanar spacing of  $(-101)$  and  $(130)$  as a function of the temperature during *in situ* XRD of pure m- $\text{Ag}_2\text{CO}_3$  under  $\text{CO}_2$  atmosphere ( $P \approx 1$  atm) up to its structural transformation; (b) projection of the structure of the monoclinic phase plotted with the CARINE crystallography software showing that the plane  $(-101)$  makes an angle of about  $10^\circ$  with the plane  $\pi$  whose normal is in the direction of the most intense thermal agitation of oxygen and silver atoms.

upon its transformation into the  $\beta$  phase [39]. This corresponds to an increase of the lattice distance  $(-101)$  induced by the temperature increase (Fig. 2a). Fig. 2b is a projection perpendicular to the bc plane of the crystal structure of m- $\text{Ag}_2\text{CO}_3$  plotted with the CARINE crystallography software. The  $\pi$  plane passing through oxygen atoms of the carbonates is represented. According to Masse et al. [56], the thermal agitation of both oxygen and silver atoms is very anisotropic and the most intense vibration is perpendicular to this  $\pi$  plane. Interestingly it makes an angle of only about  $10^\circ$  with the  $(-101)$  plane. It follows that the highly anisotropic thermal vibrations of O and Ag atoms during the temperature increase, which are perpendicular to the  $\pi$  plane, also tend to separate the  $(-101)$  planes, as shown in Fig. 2. This process facilitates the phase transformation and must require a low energy, which would explain the sensitivity to the synthesis protocol.

### 3.2. Photocatalytic properties in the visible light

The photocatalytic activity of pure  $\text{Ag}_2\text{CO}_3$  is well known [30,32,57]. As preliminary experiment the activity of as-prepared Pal- $\text{Ag}_2\text{CO}_3$ -1h nanocomposite sample synthesized according to protocol 1 was first analyzed using the tests described in the experimental section. Fig. 3 confirms that the composite Pal-57% $\text{Ag}_2\text{CO}_3$ -1h is an active photocatalyst both under UV and Visible light. This demonstrates that palygorskite is a very good support material for photocatalysis, even for

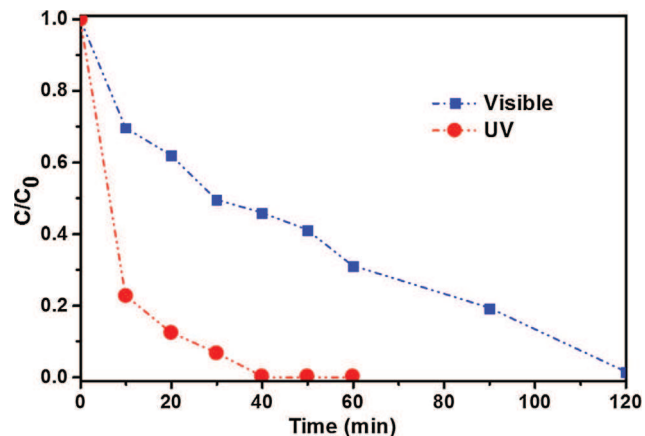


Fig. 3. Photocatalytic OG conversion under UV (●) and Visible (■) light as a function of the irradiation time for as-prepared Pal-57% $\text{Ag}_2\text{CO}_3$ -1h nanocomposite. The synthesis was made according to protocol 1.  $C_0$  and  $C$  are OG concentrations at  $t = 0$  and after an irradiation time  $t$ , respectively.

photo-activity induced by the visible light. Indeed, palygorskite was already found as a suitable support in UV photocatalysis using Pal/ $\text{TiO}_2$  nanocomposite material [25,46] but because undoped titania is inactive under visible irradiation no test was done in the visible-light range. Because the photocatalysis under visible light is more sensitive to electronic properties of the semiconductor, one could fear that a support material of rather complex composition as a clay mineral, containing many cations and anions, was not a suitable surface because of the risks of contamination of  $\text{Ag}_2\text{CO}_3$  NPs by uncontrolled self-doping that could be traps for the charge carriers. The high activity observed in the visible light for the composite reveals this does not occur.

In the Pal-57 wt% $\text{Ag}_2\text{CO}_3$ -1h sample investigated here, the active component  $\text{Ag}_2\text{CO}_3$  is present both in the monoclinic (39%) and hexagonal  $\beta$  (18%) forms, as reported in the previous companion article [39]. The OG decomposition rate can be fitted with a first order law whose the rate constant, assessed from the slope of  $\ln(C/C_0)$  versus irradiation time ranging from 0 to 30 min upon UV irradiation and from 0 to 90 min under visible light illumination, is significantly higher under UV ( $0.10 \text{ min}^{-1}$ ) than under visible ( $0.02 \text{ min}^{-1}$ ) light, as generally observed for other photocatalysts. Even under visible light a total decomposition is observed after 2 h, which is only 3 times longer than under UV irradiation. After this first series of experiments, only visible tests were performed with other photocatalysts because their main interest is effectively a high activity in the daylight. It is worth noting that under test conditions, and in both cases, OG decomposition curves do not tend toward a plateau, indicating that the dye decomposition continues and therefore no poisoning effect of the  $\text{Ag}_2\text{CO}_3$  photocatalyst surface or its premature decomposition occurred, for instance by photocorrosion.

The photocatalytic activity of different samples has been tested under visible light for the degradation of OG in aqueous solution (Fig. 4). The pristine palygorskite  $\text{Na}^+$ -Pal sample has no noticeable effect to reduce the OG concentration. This means there is no photocatalytic activity as expected since there is no component known to exhibit such property in this natural clay material. This means also that adsorption of this model pollutant is negligible on palygorskite as already demonstrated by Bouna et al. [25,44].

By contrast, evidence for visible photocatalytic activity of pure  $\text{Ag}_2\text{CO}_3$  exhibiting a structure 100% monoclinic is shown by a continuous degradation of the model dye pollutant (Fig. 4). A decrease of its concentration is observed for about 1 h at a rate around  $7 \times 10^{-3} \text{ min}^{-1}$ , which is approximately 10 times lower than that of the composite Pal-57% $\text{Ag}_2\text{CO}_3$ -1h. In addition, the degradation rate tends toward a threshold beyond 90 min leaving about 40% of OG in the aqueous solution after 2 h whereas a complete removal of the

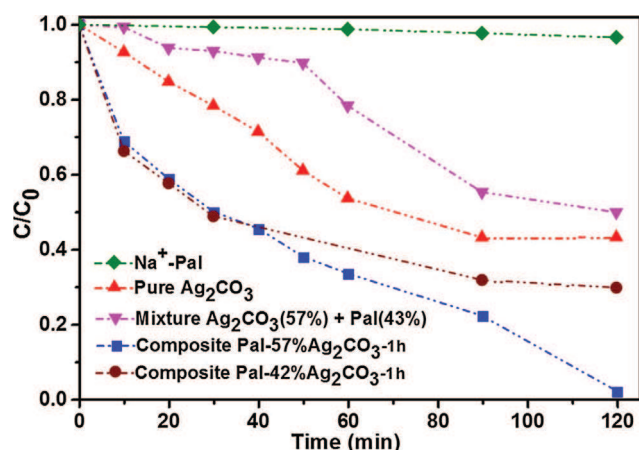


Fig. 4. OG conversion rate under visible light as a function of irradiation time. Data are reported for  $\text{Na}^+$ -exchanged palygorskite ( $\text{Na}^+$ -Pal), pure  $\text{m-Ag}_2\text{CO}_3$ , the supported nanocomposites Pal-42% $\text{Ag}_2\text{CO}_3$ -1h and Pal-57% $\text{Ag}_2\text{CO}_3$ -1h synthesized according to protocol 1, and a simple crushed mixture of  $\text{Ag}_2\text{CO}_3$  and palygorskite containing 57 wt%  $\text{Ag}_2\text{CO}_3$ . The sample amount used for pure  $\text{m-Ag}_2\text{CO}_3$  was 14.25 mg. The quantity used for the last 3 samples was 25 mg including 14.25 mg of  $\text{Ag}_2\text{CO}_3$  for the composite Pal-57% $\text{Ag}_2\text{CO}_3$ -1h and the crushed mixture, whereas only 10.5 mg were used for the composite Pal-42% $\text{Ag}_2\text{CO}_3$ -1h.

pollutant is obtained with Pal-57% $\text{Ag}_2\text{CO}_3$ -1h over the same period. The behavior of pure  $\text{Ag}_2\text{CO}_3$  could be due to a poisoning effect by the by-products of the OG decomposition or to photo-corrosion effect (not investigated at this stage).

Regarding the behavior of Pal- $\text{Ag}_2\text{CO}_3$  nanocomposite materials, OG photocatalytic degradation clearly increases with the increase of  $\text{Ag}_2\text{CO}_3$  content as shown by the samples Pal-42% $\text{Ag}_2\text{CO}_3$ -1h and Pal-57% $\text{Ag}_2\text{CO}_3$ -1h (both prepared according to protocol 1) containing 10.5 and 14.25 mg of  $\text{Ag}_2\text{CO}_3$ , respectively. Indeed, OG degradation curves for Pal-57% $\text{Ag}_2\text{CO}_3$ -1h and Pal-42% $\text{Ag}_2\text{CO}_3$ -1h are superposed during the first 40 min indicating that initial OG degradation rate is the same for both photocatalysts (reduction of approximately 55%). Beyond this period, the photocatalytic activity of Pal-42% $\text{Ag}_2\text{CO}_3$ -1h tends to a threshold at 30% while a complete removal is obtained with Pal-57% $\text{Ag}_2\text{CO}_3$ -1h after 2 h. The difference of photocatalytic efficiency of the two composites is certainly due to the different contents of  $\text{Ag}_2\text{CO}_3$ .

To check if  $\text{Ag}_2\text{CO}_3$  content in the nanocomposite is the only feature that influences the photocatalytic activity, a new sample, containing the same amount of  $\text{Ag}_2\text{CO}_3$  (57 wt%) and Pal (43 wt%), was prepared as a simple mixture coarsely ground in an agate mortar of  $\text{Ag}_2\text{CO}_3$  (100% monoclinic) and palygorskite. It exhibited a significantly lower photocatalytic activity with respect to the synthesized nanocomposite Pal-57% $\text{Ag}_2\text{CO}_3$ -1h that has the same chemical composition, as revealed by the lower initial degradation rate and the 40% of dye left in the solution after 2 h of irradiation (Fig. 4). This difference could be ascribed to the difference of  $\text{Ag}_2\text{CO}_3$  particles size between the two samples since in the case of the nanocomposite, the particles size has been found smaller than in the mixture sample as described in the previous companion paper [39]. However the different crystal structure of  $\text{Ag}_2\text{CO}_3$  may also be a key feature to account for this behavior since the silver carbonate was 100% monoclinic in the sample consisting of a mixture of powders whereas in the synthesized nanocomposite both phases m- and  $\beta$ - $\text{Ag}_2\text{CO}_3$  were present in proportions of about 70% m and 30%  $\beta$  (Table 2). This result strongly supports the great interest in supporting  $\text{Ag}_2\text{CO}_3$  on palygorskite fibers, first to stabilize the metastable hexagonal  $\beta$ -phase, secondly to decrease the average size of the active particles to the nanometric scale, and subsequently to produce more efficient supported photocatalysts.

The comparison of the efficiency of photocatalysts is always difficult

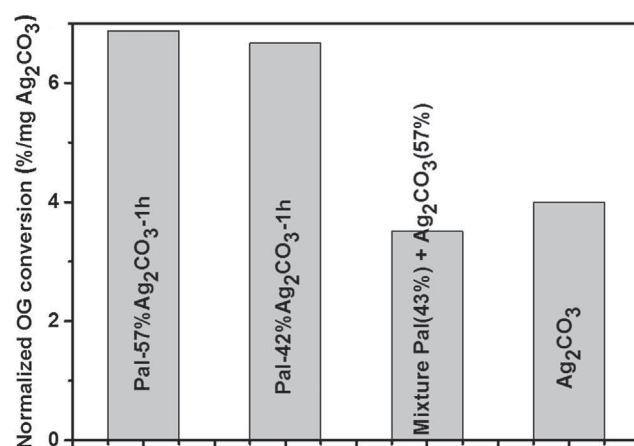


Fig. 5. Comparison of photocatalytic OG conversion rate under visible light at 120 min normalized by the mass of the active photocatalyst ( $\text{Ag}_2\text{CO}_3$ ) for different samples.

because of the many parameters which affect this property, in particular the amount of active photocatalyst. An attempt has been made in Fig. 5 for the photocatalysts investigated in this work because the same synthesis method and photocatalytic test were used. This Fig. 5 shows the OG conversion rate at 120 min measured in the visible photocatalytic tests normalized by the mass of  $\text{Ag}_2\text{CO}_3$  present in each sample. The two Pal- $\text{Ag}_2\text{CO}_3$  composites are more efficient than pure  $\text{Ag}_2\text{CO}_3$  and the simple crushed mixture of  $\text{Ag}_2\text{CO}_3$  with palygorskite. These data also confirm that the photoactivity increases with the content of  $\text{Ag}_2\text{CO}_3$  immobilized onto palygorskite fibers of the composite material. The sample Pal-57% $\text{Ag}_2\text{CO}_3$ -1h is the most efficient photocatalyst: it is only slightly more efficient than Pal-42% $\text{Ag}_2\text{CO}_3$ , but it allows removing 1.7 times more OG than pure  $\text{Ag}_2\text{CO}_3$  and 2 times more than the simple crushed mixture of  $\text{Ag}_2\text{CO}_3$  with palygorskite.

At this stage the question of the photocatalytic activity of the metastable hexagonal  $\beta$ - $\text{Ag}_2\text{CO}_3$  phase compared with that of the stable monoclinic phase becomes particularly interesting. To address this issue, photocatalytic tests were performed on different Pal-57% $\text{Ag}_2\text{CO}_3$  composite materials. The first one was elaborated according to protocol 2 (Pal-57% $\text{Ag}_2\text{CO}_3$ -24h) and it contained 100% of monoclinic  $\text{m-Ag}_2\text{CO}_3$ . A second sample was freshly synthesized according to protocol 1 (Pal-57% $\text{Ag}_2\text{CO}_3$ -1h) and it contained a mixture of about 32 wt% of  $\beta$ - and 68 wt% of  $\text{m-Ag}_2\text{CO}_3$  as reported in Table 2. The last composite of this series was obtained by the protocol 3, i.e. it was synthesized following protocol 1, then it was aged for 6 months in dark and it underwent a thermal cycle at 200 °C under  $\text{CO}_2$  for 1 h before returning to room temperature. Under these conditions the composite sample exhibits 100% of hexagonal  $\beta$ - $\text{Ag}_2\text{CO}_3$ .

Fig. 6 shows OG conversion rate under visible light as a function of the irradiation time for the three Pal-57% $\text{Ag}_2\text{CO}_3$  nanocomposite samples; they contain the same total amount of  $\text{Ag}_2\text{CO}_3$  (57 wt%), but the relative content of metastable hexagonal  $\beta$ - $\text{Ag}_2\text{CO}_3$  is 0, 32 and 100%. The two nanocomposite samples containing a single-phase  $\text{Ag}_2\text{CO}_3$ , i.e. 100%  $\beta$ -hexagonal or 100% monoclinic have approximately the same OG degradation rate during the first hour of the test. Beyond one hour, the supported nanocomposite containing 100%  $\text{m-Ag}_2\text{CO}_3$  exhibits a better activity than the composite containing 100%  $\beta$ - $\text{Ag}_2\text{CO}_3$ . Thus, after 2 h, the reduction of OG concentration in the aqueous solution is 75% and 40% respectively. For both samples, the degradation over 2 h is continuous without a plateau being reached. The degradation rate is relatively slow and more time is required for a complete decomposition; a rough extrapolation leads to approximately 2.6 h and 5.3 h, respectively.

A different behavior is observed for the bi-phased (m +  $\beta$ )- $\text{Ag}_2\text{CO}_3$ /Pal nanocomposite containing 32% of  $\beta$ -hexagonal and 68% of

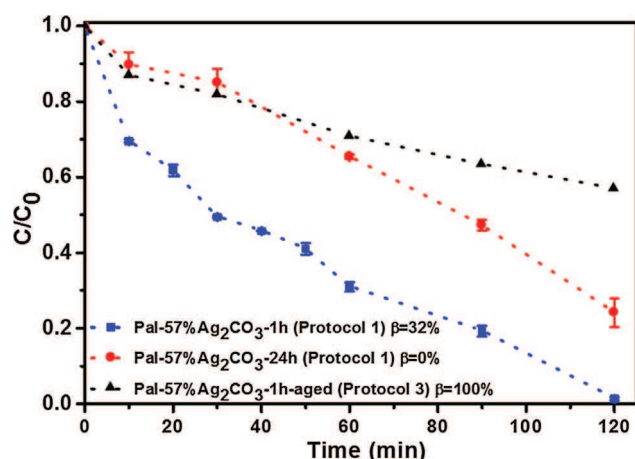


Fig. 6. OG conversion rate under visible light as a function of the irradiation time. Data are reported for three Pal-57 wt%Ag<sub>2</sub>CO<sub>3</sub> supported nanocomposite samples where the relative content of β-Ag<sub>2</sub>CO<sub>3</sub> was 0% (protocol 2), 32% (protocol 1) and 100% (protocol 3). The total mass of analyzed sample was 25 mg, including 14.25 mg of total amount of Ag<sub>2</sub>CO<sub>3</sub>.

monoclinic. For this sample the initial degradation rate is significantly higher, approximately 2.5 faster than for the single-phased Ag<sub>2</sub>CO<sub>3</sub>/Pal nanocomposites. Furthermore the OG photocatalytic decomposition is complete in only 2 h while a large proportion is not yet degraded using the two single-phased Ag<sub>2</sub>CO<sub>3</sub>/Pal nanocomposites. The higher efficiency of the bi-phased (m + β)-Ag<sub>2</sub>CO<sub>3</sub>/Pal nanocomposite is likely the result of a synergetic effect between the two active phases as this was reported for several couples as anatase-rutile [58], Ag<sub>2</sub>O/Ag<sub>2</sub>CO<sub>3</sub> [59] and AgX/Ag<sub>3</sub>PO<sub>4</sub> [60].

The high visible-light photocatalytic activity of the stable phase m-Ag<sub>2</sub>CO<sub>3</sub> is due to its suitable indirect band gap semiconductor reported to be, depending on the synthesis method, 2.08 eV [61], 2.30 eV [29], 2.34 eV [55] and 2.46 eV [55]. Unfortunately, no data was found about the electronic structure (energy band gap) of the metastable β-Ag<sub>2</sub>CO<sub>3</sub> phase. Consequently, we cannot comment more the beneficial effect that significantly improves the photocatalytic properties of these new Ag<sub>2</sub>CO<sub>3</sub>/Pal supported nanocomposite materials. However the two phases of Ag<sub>2</sub>CO<sub>3</sub> (m and β) originate from different reaction pathways in the overall growth mechanism [39] and heterojunctions between these two types of nanoparticles should exist. They could then play a key role as in some couples of photocatalysts like g-C<sub>3</sub>N<sub>4</sub>/Ag<sub>2</sub>CO<sub>3</sub> [48].

#### 4. Conclusions

This study has demonstrated that the new Pal-Ag<sub>2</sub>CO<sub>3</sub> supported nanocomposite exhibits an efficient visible photocatalytic activity, which increases with the total amount of Ag<sub>2</sub>CO<sub>3</sub> in the sample. Furthermore, the nanocomposite material containing 57 wt% of Ag<sub>2</sub>CO<sub>3</sub> was found more active than pure Ag<sub>2</sub>CO<sub>3</sub>, i.e. without palygorskite as support material, and also better than a simple crushed mixture of Ag<sub>2</sub>CO<sub>3</sub> and palygorskite. This denotes the great interest of developing supported photocatalysts based on clay minerals, which besides present the advantage to flocculate easily making their recovering from treated waste water easy without resorting to expensive microfiltration. In addition, Pal/Ag<sub>2</sub>CO<sub>3</sub> nanocomposite materials in which Ag<sub>2</sub>CO<sub>3</sub> crystallizes entirely either in the metastable hexagonal β-structure or in the stable monoclinic structure exhibit similar photocatalytic activity over approximately one hour, but beyond this period the monoclinic based composite showed a better activity than the hexagonal one. Nevertheless, the most striking result is that they remain significantly less photoactive than nanocomposites in which Ag<sub>2</sub>CO<sub>3</sub> exists in both crystal structure with 32% of β-phase and 68% of m-phase. This improvement is ascribed to synergetic effect between

both phases as reported for anatase-rutile, g-C<sub>3</sub>N<sub>4</sub>/Ag<sub>2</sub>CO<sub>3</sub> [48] and other couples of photocatalysts. The role of palygorskite is essential to stabilize the metastable β-phase, which allows obtaining this synergetic effect. The long-term behavior is under study, and therefore the photocorrosion of these new photocatalysts will be discussed in a future paper.

#### Acknowledgement

The financial supports from the “Programme d'Action Intégrée Volubilis” (N° 14/SM/14) and the Project of PPR-CNRST “Domaines Prioritaires de la Recherche Scientifique et du Développement Technologique” (PPR1/2015/63) are gratefully acknowledged.

#### References

- [1] O. Carp, Photoinduced reactivity of titanium dioxide, *Prog. Solid State Chem.* 32 (2004) 33–177, <https://doi.org/10.1016/j.progsolidstchem.2004.08.001>.
- [2] J. Herrmann, Heterogeneous photocatalysis: fundamentals and applications to the removal of various types of aqueous pollutants, *Catal. Today* 53 (1999) 115–129, [https://doi.org/10.1016/S0920-5861\(99\)00107-8](https://doi.org/10.1016/S0920-5861(99)00107-8).
- [3] M. Nieto-Suárez, G. Palmisano, M.L. Ferrer, M.C. Gutiérrez, S. Yurdakal, V. Augugliaro, M. Pagliaro, F. del Monte, Self-assembled titania-silica-sepiolite based nanocomposites for water decontamination, *J. Mater. Chem.* 19 (2009) 2070, <https://doi.org/10.1039/b813864h>.
- [4] M. Houari, M. Saidi, D. Tabet, P. Pichat, H. Khalaf, The removal of 4-chlorophenol and dichloroacetic acid in water using Ti-, Zr- and Ti/Zr-pillared bentonites as photocatalyst, *Am. J. Appl. Sci.* 2 (2005) 1136–1140, <https://doi.org/10.3844/ajassp.2005.1136.1140>.
- [5] J. Liu, M. Dong, S. Zuo, Y. Yu, Solvothermal preparation of TiO<sub>2</sub>/montmorillonite and photocatalytic activity, *Appl. Clay Sci.* 43 (2009) 156–159, <https://doi.org/10.1016/j.clay.2008.07.016>.
- [6] K.R. Kunduru, M. Nazarkovsky, S. Farah, R.P. Pawar, A. Basu, A.J. Domb, Nanotechnology for water purification: applications of nanotechnology methods in wastewater treatment, *Water Purif.* (2017) 33–74, <https://doi.org/10.1016/B978-0-12-804300-4.00002-2>.
- [7] D. Robert, A. Piscopo, O. Heintz, J.V. Weber, Photocatalytic detoxification with TiO<sub>2</sub> supported on glass-fibre by using artificial and natural light, *Catal. Today* 54 (1999) 291–296, [https://doi.org/10.1016/S0920-5861\(99\)00190-X](https://doi.org/10.1016/S0920-5861(99)00190-X).
- [8] B. Siffert, J. Metzger, Study of the interaction of titanium dioxide with cellulose fibers in an aqueous medium, *Coll. Surf.* 53 (1991) 79–99, [https://doi.org/10.1016/0166-6622\(91\)80037-O](https://doi.org/10.1016/0166-6622(91)80037-O).
- [9] S.C. Jung, B.H. Kim, S.J. Kim, N. Imaishi, Y.I. Cho, Characterization of a TiO<sub>2</sub> photocatalyst film deposited by CVD and its photocatalytic activity, *Chem. Vap. Depos.* 11 (2005) 137–141, <https://doi.org/10.1002/cvde.200406321>.
- [10] J. Gijlalaj, I. Alessandri, Easy recovery, mechanical stability, enhanced adsorption capacity and recyclability of alginate-based TiO<sub>2</sub> macrobead photocatalysts for water treatment, *J. Environ. Chem. Eng.* 5 (2017) 1763–1770, <https://doi.org/10.1016/j.jece.2017.03.017>.
- [11] C.S. Kim, I.M. Kwon, B.K. Moon, J.H. Jeong, B.C. Choi, J.H. Kim, H. Choi, S.S. Yi, D.H. Yoo, K.S. Hong, J.H. Park, H.S. Lee, Synthesis and particle size effect on the phase transformation of nanocrystalline TiO<sub>2</sub>, *Mater. Sci. Eng. C* 27 (2007) 1343–1346, <https://doi.org/10.1016/j.msec.2006.12.006>.
- [12] W. Aloulou, W. Hamza, H. Aloulou, A. Oun, S. Khemakhem, A. Jada, S. Chakraborty, S. Curcio, R. Ben Amar, Developing of titania-smectite nanocomposites UF membrane over zeolite based ceramic support, *Appl. Clay Sci.* 155 (2018) 20–29, <https://doi.org/10.1016/j.clay.2017.12.035>.
- [13] C. Sarantopoulos, A.N. Gleizes, F. Maury, Chemical vapor infiltration of photocatalytically active TiO<sub>2</sub> thin films on glass microfibers, *Surf. Coat. Technol.* 201 (2007) 9354–9358, <https://doi.org/10.1016/j.surfcoat.2007.04.073>.
- [14] C. Sarantopoulos, E. Puzenat, C. Guillard, J.-M. Herrmann, A.N. Gleizes, F. Maury, Microfibrillar TiO<sub>2</sub> supported photocatalysts prepared by metal-organic chemical vapor infiltration for indoor air and waste water purification, *Appl. Catal. B Environ.* 91 (2009) 225–233, <https://doi.org/10.1016/j.apcatb.2009.05.029>.
- [15] X.Y. Chuan, M. Hirano, M. Inagaki, Preparation and photocatalytic performance of anatase-mounted natural porous silica, pumice, by hydrolysis under hydrothermal conditions, *Appl. Catal. B Environ.* 51 (2004) 255–260, <https://doi.org/10.1016/j.apcatb.2004.03.004>.
- [16] H.P. Kuo, S.W. Yao, A.N. Huang, W.Y. Hsu, Photocatalytic degradation of toluene in a staged fluidized bed reactor using TiO<sub>2</sub>/silica gel, *Kor. J. Chem. Eng.* 34 (2017) 73–80, <https://doi.org/10.1007/s11814-016-0248-6>.
- [17] E.P. Reddy, L. Davydov, P. Smirniotis, TiO<sub>2</sub>-loaded zeolites and mesoporous materials in the sonophotocatalytic decomposition of aqueous organic pollutants: The role of the support, *Appl. Catal. B Environ.* 42 (2003) 1–11, [https://doi.org/10.1016/S0926-3373\(02\)00192-3](https://doi.org/10.1016/S0926-3373(02)00192-3).
- [18] S. Nagaoka, Y. Hamasaki, S.-I. Ishihara, M. Nagata, K. Iio, C. Nagasawa, H. Ihara, Preparation of carbon/TiO<sub>2</sub> microsphere composites from cellulose/TiO<sub>2</sub> microsphere composites and their evaluation, *J. Mol. Catal. A Chem.* 177 (2002) 255–263, [https://doi.org/10.1016/S1381-1169\(01\)00271-0](https://doi.org/10.1016/S1381-1169(01)00271-0).
- [19] B. Herbig, P. Löbmann, TiO<sub>2</sub> photocatalysts deposited on fiber substrates by liquid phase deposition, *J. Photochem. Photobiol. A Chem.* 163 (2004) 359–365, <https://doi.org/10.1016/j.jphotochem.2004.03.004>.



[doi.org/10.1016/j.jphotochem.2004.01.005](https://doi.org/10.1016/j.jphotochem.2004.01.005).

- [20] T. An, J. Chen, G. Li, X. Ding, G. Sheng, J. Fu, B. Mai, K.E. O'Shea, Characterization and the photocatalytic activity of TiO<sub>2</sub> immobilized hydrophobic montmorillonite photocatalysts. Degradation of decabromodiphenyl ether (BDE 209), *Catal. Today* 139 (2008) 69–76, <https://doi.org/10.1016/j.cattod.2008.08.024>.
- [21] P. Aranda, R. Kun, M.A. Martín-Luengo, S. Letaief, I. Dékány, E. Ruiz-Hitzky, Titania–sepiolite nanocomposites prepared by a surfactant templating colloidal route, *Chem. Mater.* 20 (2008) 84–91, <https://doi.org/10.1021/cm702251f>.
- [22] J. Feng, X. Hu, P.L. Yue, H.Y. Zhu, G.Q. Lu, A novel laponite clay-based Fe nanocomposite and its photo-catalytic activity in photo-assisted degradation of Orange II, *Chem. Eng. Sci.* 58 (2003) 679–685, [https://doi.org/10.1016/S0009-2509\(02\)00595-X](https://doi.org/10.1016/S0009-2509(02)00595-X).
- [23] G. Zhang, Q. Xiong, W. Xu, S. Guo, Synthesis of bicrystalline TiO<sub>2</sub> supported sepiolite fibers and their photocatalytic activity for degradation of gaseous formaldehyde, *Appl. Clay Sci.* 102 (2014) 231–237, <https://doi.org/10.1016/j.clay.2014.10.001>.
- [24] F. Zhou, C. Yan, H. Wang, S. Zhou, S. Komarneni, Sepiolite-TiO<sub>2</sub> nanocomposites for photocatalysis: Synthesis by microwave hydrothermal treatment versus calcination, *Appl. Clay Sci.* 146 (2017) 246–253, <https://doi.org/10.1016/j.clay.2017.06.010>.
- [25] L. Bouna, B. Rhouta, M. Amjoud, F. Maury, M.-C. Lafont, a. Jada, F. Senocq, L. Daoudi, Synthesis, characterization and photocatalytic activity of TiO<sub>2</sub> supported natural palygorskite microfibers, *Appl. Clay Sci.* 52 (2011) 301–311, <https://doi.org/10.1016/j.clay.2011.03.009>.
- [26] L. Bouna, B. Rhouta, F. Maury, A. Jada, F. Senocq, M.-C. Lafont, Photocatalytic activity of TiO<sub>2</sub>/stevensite nanocomposites for the removal of Orange G from aqueous solutions, *Clay Miner.* 49 (2014) 417–428, <https://doi.org/10.1180/claymin.2014.049.3.05>.
- [27] B. Rhouta, L. Bouna, F. Maury, F. Senocq, M.C. Lafont, A. Jada, M. Amjoud, L. Daoudi, Surfactant-modifications of Na<sup>+</sup>-beidellite for the preparation of TiO<sub>2</sub>-Bd supported photocatalysts: II—Physico-chemical characterization and photocatalytic properties, *Appl. Clay Sci.* 115 (2015) 266–274, <https://doi.org/10.1016/j.clay.2015.04.025>.
- [28] O. Lakbata, B. Rhouta, F. Maury, F. Senocq, M. Amjoud, A. Jada, Supported photocatalyst based on CuO – TiO<sub>2</sub>/palygorskite nanocomposite material for wastewater treatment, *J. Colloid Sci. Biotechnol.* 5 (2016) 1–7, <https://doi.org/10.1166/jcsb.2016.1150>.
- [29] G. Dai, J. Yu, G. Liu, A new approach for photocorrosion inhibition of Ag<sub>2</sub>CO<sub>3</sub> photocatalyst with highly visible-light-responsive reactivity, *J. Phys. Chem. C* 116 (2012) 15519–15524, <https://doi.org/10.1021/jp305669f>.
- [30] Y. Wang, P. Ren, C. Feng, X. Zheng, Z. Wang, D. Li, Photocatalytic behavior and photo-corrosion of visible-light-active silver carbonate/titanium dioxide, *Mater. Lett.* 115 (2014) 85–88, <https://doi.org/10.1016/j.matlet.2013.10.025>.
- [31] C. Feng, G. Li, P. Ren, Y. Wang, X. Huang, D. Li, Effect of photo-corrosion of Ag<sub>2</sub>CO<sub>3</sub> on visible light photocatalytic activity of two kinds of Ag<sub>2</sub>CO<sub>3</sub>/TiO<sub>2</sub> prepared from different precursors, *Appl. Catal. B: Environ.* 158–159 (2014) 224–232, <https://doi.org/10.1016/j.apcatb.2014.04.020>.
- [32] H. Xu, J. Zhu, Y. Song, T. Zhu, W. Zhao, Y. Song, Z. Da, C. Liu, H. Li, Fabrication of AgX-loaded Ag<sub>2</sub>CO<sub>3</sub> (X = Cl, I) composites and their efficient visible-light-driven photocatalytic activity, *J. Alloys Compd.* 622 (2015) 347–357, <https://doi.org/10.1016/j.jallcom.2014.09.148>.
- [33] C. Yu, L. Wei, W. Zhou, D.D. Dionysiou, L. Zhu, Q. Shu, H. Liu, A visible-light-driven core-shell like Ag<sub>2</sub>S@Ag<sub>2</sub>CO<sub>3</sub> composite photocatalyst with high performance in pollutants degradation, *Chemosphere* 157 (2016) 250–261, <https://doi.org/10.1016/j.chemosphere.2016.05.021>.
- [34] J. Tian, Z. Wu, Z. Liu, C. Yu, K. Yang, L. Zhu, W. Huang, Y. Zhou, Low-cost and efficient visible-light-driven CaMg(CO<sub>3</sub>)<sub>2</sub>@Ag<sub>2</sub>CO<sub>3</sub> microspheres fabricated via an ion exchange route, *Cuihua Xuebao/Chin. J. Catal.* 38 (2017) 1899–1908, [https://doi.org/10.1016/S1872-2067\(17\)62924-3](https://doi.org/10.1016/S1872-2067(17)62924-3).
- [35] J. Tian, R. Liu, Z. Liu, C. Yu, M. Liu, Boosting the photocatalytic performance of Ag<sub>2</sub>CO<sub>3</sub> crystals in phenol degradation via coupling with trace N-CQDs, *Cuihua Xuebao/Chin. J. Catal.* 38 (2017) 1999–2008, [https://doi.org/10.1016/S1872-2067\(17\)62926-7](https://doi.org/10.1016/S1872-2067(17)62926-7).
- [36] S. Sohrabnezhad, A. Sadeghi, Matrix effect of montmorillonite and MCM-41 matrices on the antibacterial activity of Ag<sub>2</sub>CO<sub>3</sub> nanoparticles, *Appl. Clay Sci.* 105–106 (2015) 217–224, <https://doi.org/10.1016/j.clay.2014.12.034>.
- [37] M. Chen, L. Yang, L. Zhang, Y. Han, Z. Lu, G. Qin, E. Zhang, Effect of nano/micro-Ag compound particles on the bio-corrosion, antibacterial properties and cell biocompatibility of Ti-Ag alloys, *Mater. Sci. Eng. C* 75 (2017) 906–917, <https://doi.org/10.1016/j.msec.2017.02.142>.
- [38] J. Mungkalasiri, L. Bedel, F. Emieux, A.V.-D. Cara, J. Freney, F. Maury, F.N.R. Renaud, Antibacterial properties of TiO<sub>2</sub>-Cu composite thin films grown by a one step DLICVD process, *Surf. Coatings Technol.* 242 (2014) 187–194, <https://doi.org/10.1016/j.surfcoat.2013.08.039>.
- [39] O. Lakbata, B. Rhouta, F. Maury, F. Senocq, M. Amjoud, L. Daoudi, On the key role of the surface of palygorskite fibers in the stabilization of hexagonal metastable phase of Ag<sub>2</sub>CO<sub>3</sub> supported on this clay mineral, under review in *Applied Clay Science* (manuscript number: CLAY 11524).
- [40] B. Rhouta, E. Zatile, L. Bouna, O. Lakbata, F. Maury, L. Daoudi, M.C. Lafont, M. Amjoud, F. Senocq, A. Jada, A. Ait Aghzzaf, Comprehensive physicochemical study of dioctahedral palygorskite-rich clay from Marrakech High Atlas (Morocco), *Phys. Chem. Miner.* 40 (2013) 411–424, <https://doi.org/10.1007/s00269-013-0579-3>.
- [41] A. Ait Aghzzaf, B. Rhouta, E. Rocca, A. Khalil, J. Steinmetz, A. Ait Aghzzaf, B. Rhouta, E. Rocca, A. Khalil, J. Steinmetz, Corrosion inhibition of zinc by calcium exchanged beidellite clay mineral: a new smart corrosion inhibitor, *Corros. Sci.* 80 (2014) 46–52, <https://doi.org/10.1016/j.corsci.2013.10.037>.
- [42] T. Holtzapfel, Les minéraux argileux: préparation, analyse diffractométrique et détermination, Société géologique du Nord, Publication n°12, 1985.
- [43] G.D. Nagy, J.B. Vergette, J.P. Connolly, differential thermal analysis studies on Ag<sub>2</sub>CO<sub>3</sub>, *Can. J. Chem.* 49 (1971) 3986–3993, <https://doi.org/10.1139/v71-665>.
- [44] L. Bouna, B. Rhouta, M. Amjoud, A. Jada, F. Maury, L. Daoudi, F. Senocq, Correlation between electrokinetic mobility and ionic dyes adsorption of Moroccan stevensite, *Appl. Clay Sci.* 48 (2010) 527–530, <https://doi.org/10.1016/j.clay.2010.02.004>.
- [45] K. Hofstadler, R. Bauer, S. Novalic, G. Heisler, New Reactor design for photocatalytic wastewater treatment with TiO<sub>2</sub> immobilized on fused-silica glass fibers: photomineralization of 4-chlorophenol, *Environ. Sci. Technol.* 28 (1994) 670–674, <https://doi.org/10.1021/es00053a021>.
- [46] L. Bouna, B. Rhouta, F. Maury, Physicochemical study of photocatalytic activity of TiO<sub>2</sub> supported palygorskite, *Clay Mineral* (2013, 2013,) 2–7.
- [47] S. Guo, J. Bao, T. Hu, L. Zhang, L. Yang, J. Peng, C. Jiang, Controllable synthesis porous Ag<sub>2</sub>CO<sub>3</sub> nanorods for efficient photocatalysis, *Nanoscale Res. Lett.* 10 (2015) 193, <https://doi.org/10.1186/s11671-015-0892-5>.
- [48] K. Wu, Y. Cui, X. Wei, X. Song, J. Huang, The hybridization of Ag<sub>2</sub>CO<sub>3</sub> rods with g-C<sub>3</sub>N<sub>4</sub> sheets with improved photocatalytic activity, *J. Saudi Chem. Soc.* 19 (2015) 465–470, <https://doi.org/10.1016/j.jscs.2015.07.002>.
- [49] P. Norby, R. Dinnebier, A.N. Fitch, Decomposition of silver carbonate; the crystal structure of two high-temperature modifications of Ag<sub>2</sub>CO<sub>3</sub>, *Inorg. Chem.* 41 (2002) 3628–3637 <http://www.ncbi.nlm.nih.gov/pubmed/12099865>.
- [50] Y. Sawada, N. Mizutani, M. Kato, Thermal decomposition of silver carbonate Part III. high temperature X-ray diffraction analysis, *Thermochim. Acta.* 146 (1989) 177–185, [https://doi.org/10.1016/0040-6031\(89\)87087-X](https://doi.org/10.1016/0040-6031(89)87087-X).
- [51] Y. Sawada, N. Mizutani, M. Kato, Thermal decomposition of silver carbonate, *Thermochim. Acta.* 143 (1989) 319–324, [https://doi.org/10.1016/0040-6031\(89\)85070-1](https://doi.org/10.1016/0040-6031(89)85070-1).
- [52] Y. Sawada, N. Kanou, N. Mizutani, Thermal decomposition of silver carbonate. Part 4. High pressure differential thermal analysis under an atmosphere of carbon dioxide, *Thermochim. Acta.* 183 (1991) 279–287, [https://doi.org/10.1016/0040-6031\(91\)80464-T](https://doi.org/10.1016/0040-6031(91)80464-T).
- [53] Y. Sawada, N. Watanabe, H. Henmi, N. Mizutani, M. Kato, Thermal decomposition of silver carbonate, *Thermochim. Acta.* 138 (1989) 257–265, [https://doi.org/10.1016/0040-6031\(89\)87262-4](https://doi.org/10.1016/0040-6031(89)87262-4).
- [54] Y. Sawada, K. Manabe, Thermal decomposition of silver carbonate, *J. Therm. Anal.* 37 (1991) 1657–1663, <https://doi.org/10.1007/BF01912194>.
- [55] H. Dong, G. Chen, J. Sun, C. Li, Y. Yu, D. Chen, A novel high-efficiency visible-light sensitive Ag<sub>2</sub>CO<sub>3</sub> photocatalyst with universal photodegradation performances: Simple synthesis, reaction mechanism and first-principles study, *Appl. Catal. B Environ.* 134–135 (2013) 46–54, <https://doi.org/10.1016/j.apcatb.2012.12.041>.
- [56] R. Masse, J.C. Guitel, A. Durif, Structure du carbonate d'argent, *Acta Crystallogr. Sect. B Struct. Crystallogr. Cryst. Chem.* 35 (1979) 1428–1429, <https://doi.org/10.1107/S0567740879006592>.
- [57] Y. Song, J. Zhu, H. Xu, C. Wang, Y. Xu, H. Ji, K. Wang, Q. Zhang, H. Li, Synthesis, characterization and visible-light photocatalytic performance of Ag<sub>2</sub>CO<sub>3</sub> modified by graphene-oxide, *J. Alloys Compd.* 592 (2014) 258–265, <https://doi.org/10.1016/j.jallcom.2013.12.228>.
- [58] J. Zhang, Q. Xu, Z. Feng, M. Li, C. Li, Importance of the relationship between surface phases and photocatalytic activity of TiO<sub>2</sub>, *Angew. Chemie - Int. Ed.* 47 (2008) 1766–1769, <https://doi.org/10.1002/anie.200704788>.
- [59] C. Yu, G. Li, S. Kumar, K. Yang, R. Jin, Phase transformation synthesis of novel Ag<sub>2</sub>O/Ag<sub>2</sub>CO<sub>3</sub> heterostructures with high visible light efficiency in photocatalytic degradation of pollutants, *Adv. Mater.* 26 (2014) 892–898, <https://doi.org/10.1002/adma.201304173>.
- [60] Y. Bi, S. Ouyang, J. Cao, J. Ye, Facile synthesis of rhombic dodecahedral AgX/Ag<sub>3</sub>PO<sub>4</sub> (X = Cl, Br, I) heterocrystals with enhanced photocatalytic properties and stabilities, *Phys. Chem. Chem. Phys.* 13 (2011) 10071, <https://doi.org/10.1039/c1cp20488b>.
- [61] C. Xu, Y. Liu, B. Huang, H. Li, X. Qin, X. Zhang, Y. Dai, Preparation, characterization, and photocatalytic properties of silver carbonate, *Appl. Surf. Sci.* 257 (2011) 8732–8736, <https://doi.org/10.1016/j.apsusc.2011.05.060>.